RSC Applied Interfaces

ROYAL SOCIETY OF CHEMISTRY

PAPER

View Article Online
View Journal | View Issue

Cite this: *RSC Appl. Interfaces*, 2025, **2**, 243

Analysis of interactions between amino acids and monolayers of charged side chains†

Akira Nomoto,[ab] Kentaro Shiraki[a] and Tsukuru Minamiki *[bc]

Protein–protein interactions (PPIs) are regulated by multiple interactions among amino acids. However, the contribution of individual amino acid–amino acid interactions (AAIs) in PPIs is currently unclear because it is difficult to analyze the weak and nonspecific interactions among amino acids. Therefore, we constructed a quantitative analytical model to evaluate AAIs using a device with self-assembled monolayers (SAMs). We could evaluate the μM-order dissociation constant between amino acids and the side chain of amino acids based on the electrical response. In the cationic amino acid group, concentration-dependent responses were observed on a negatively charged SAM (3-mercaptopropionic acid). These responses were modulated by the concentration and valence of the competing ions, which indicated that the strength of electrostatic interactions among amino acids is different. In contrast, nonspecific responses to all amino acids used in this study were obtained on a positively charged SAM (2-mercaptoethylamine). These results indicate that the selectivity of interaction depends on the type of side chain in the assembled state. We believe that the analytical platform constructed in this study can be adapted to evaluate various AAIs that govern PPIs.

Received 3rd September 2024,
Accepted 15th November 2024

DOI: 10.1039/d4lf00310a

rsc.li/RSCApplInter

Introduction

Protein–protein interactions (PPIs), known as macromolecular interactions between homologous or heterologous proteins, drive the formation of supra-organizations of proteins, such as nanometer-sized complexes and micrometer-sized assemblies.[1,2] Protein assemblies formed by phase separation regulate complex biological reactions (*e.g.*, signalling, metabolism, *etc.*).[3] PPI analysis is also critical for industries dependent on proteins, such as those involved in the development of enzymatic biomass and drug discovery.[4,5] PPIs include specific interactions through structural subunits and nonspecific interactions, such as electrostatic interactions, hydrogen bonding, and hydrophobic interactions, resulting from multiple interactions among amino acids.[6,7] Therefore, for desired control of PPIs, it is critical to understand amino acid–amino acid interactions (AAIs) at the molecular level.

PPIs mediated by structural domains or small molecules have been evaluated using various analytical methods.[8] For example, changes in PPIs induced by thermal and electromagnetic radiation are analyzed using *in vitro* methods.[9,10] In *in vivo* methods, PPIs are examined based on changes in fluorescence intensity of labeling probes and transcriptional activity.[11,12] In addition, computational approaches are employed to predict PPIs using *in silico* modeling and simulations based on sequence and structure information.[13] Consequently, a tremendous amount of knowledge on macro- and mesoscopic interactions of proteins has accumulated, and several databases for such interactions have been created.[14,15] However, the microscopic contributions of each AAI in governing PPIs remain unclear.[7] Although computational approaches have been devised to unravel individual interactions between single amino acid molecules,[16] experimental analysis of such interactions is still in its infancy. In conventional methods for analyzing molecular interactions, the determination of individual AAIs in a protein assembly is challenging,[17] meaning that the analysis of weak and nonspecific interactions between individual amino acids is difficult using the above-mentioned approaches for evaluating PPIs. Hence, the development of analytical methods for weak molecular interactions of amino acids is desirable.

The use of self-assembled monolayers (SAMs) is one of the key approaches to evaluate intermolecular interactions because they provide the reaction field in which the molecules assemble.[18] SAM systems can be applied to model

[a] *Faculty of Pure and Applied Sciences, University of Tsukuba, 1-1-1 Tennodai, Tsukuba, Ibaraki 305-8573, Japan*
[b] *Health and Medical Research Institute, National Institute of Advanced Industrial Science and Technology (AIST), 1-1-1 Higashi, Tsukuba, Ibaraki 305-8566, Japan. E-mail: t.minamiki@aist.go.jp*
[c] *Precursory Research for Embryonic Science and Technology (PRESTO), Japan Science and Technology Agency (JST), 4-1-8 Honcho, Kawaguchi, Saitama 332-0012, Japan*

† Electronic supplementary information (ESI) available: Analysis details of output voltage and self-assembled monolayers. See DOI: https://doi.org/10.1039/d4lf00310a

biological responses modulated by specific host–guest interactions, such as catalytic reactions and immunoassays.[19,20] Moreover, by introducing artificial receptors into SAMs, small molecules such as sugars, ions and biogenic amines can also be detected.[21–23] Therefore, SAMs can detect not only specific reactions triggered by macromolecules, but also weak molecular interactions between small molecules. In particular, SAM systems combined with field-effect transistors (FETs) are on-site sensing platforms that enable high throughput and sensitivity of analyte detection due to their integration capability and electrochemical detection mechanism.[23,24] In light of these findings, we propose that FETs modified by SAMs with amino acid functional groups could be considered as substructural models of proteins and used to detect weak molecular interactions between amino acids.

Mutations in charged amino acids in proteins can dramatically alter PPIs, affecting the function, solubility, and assembly state of proteins.[25,26] Hence, understanding the contribution of individual AAIs between charged amino acids expands the potential applications of proteins in various industries. In this study, we constructed a quantitative analysis system using a FET-based sensor modified with different surface charges composed of two types of amino acid side-chain mimicking monolayers. We then evaluated the AAIs between charged amino acids in solution and the side chain on SAMs by measuring the electrical response. Finally, we investigated the influence of ionic strength in solution on AAIs to understand the mode of electrostatic AAIs in detail. Using SAM systems, we have successfully analyzed the differences in the strength of AAIs as a function of solution conditions and amino acid species.

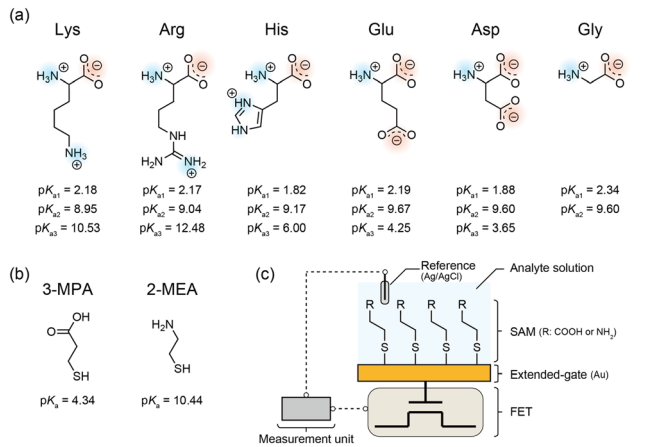

Fig. 1 Chemical structures of (a) amino acid analytes and (b) monomers used for preparing self-assembled monolayers (SAMs) mimicking the electrically charged side chains examined in this study. The described pK_a values (a1, α-carboxyl group; a2, α-amino group; a3, side chain) were referred from previous studies.[27–29] (c) Schematic illustration of a field-effect transistor (FET) sensor functionalized with a SAM, mimicking the amino acid side chains.

Experimental details

Materials

To evaluate AAIs, we used L-lysine (Lys), L-arginine (Arg), L-histidine (His), L-glutamic acid (Glu), L-aspartic acid (Asp), and glycine (Gly) as analytes (Fig. 1a). Lys, Arg, His, Glu, Asp, calcium chloride ($CaCl_2$), and dimethyl sulfoxide (DMSO) were purchased from Wako Pure Chemical Industries, Ltd. (Osaka, Japan). Gly, isopropyl alcohol (IPA), and sodium chloride (NaCl) were purchased from Kanto Chemical Co., Inc. (Tokyo, Japan). 3-Mercaptopropionic acid (3-MPA) and 2-mercaptoethylamine (2-MEA), used as self-assembled monolayer (SAM) monomers (Fig. 1b), were purchased from Tokyo Chemical Industry Co., Ltd. (Tokyo, Japan). 3-Morpholinopropanesulfonic acid (MOPS) was purchased from Sigma-Aldrich (St. Louis, MO, USA). The buffer solutions were prepared in Milli-Q water (18 MΩ cm resistivity at 25 °C). All the reagents utilized in this study were used as supplied.

Functionalization of FET-based sensors

We utilized an on-chip sensor array chip consisting of 64 × 64 extended-gate type FETs. All FET devices were equipped with a gold (Au) extended-gate electrode (BC2, BioCMOS Co., Ltd.). Because the sensing part (the extended-gate) and transducing unit (the FET channel) in the FET sensor are separated, repeatable and stable measurements of analytes in aqueous solutions are ensured by the extended-gate configuration of the FETs (Fig. 1c). Before functionalization of the FET devices, the surface of the Au extended-gate electrodes was first rinsed with IPA and Milli-Q water. The electrodes were then cleaned by vacuum plasma treatment for 1 min (introduced gas: atmospheric air). The Au electrodes were immersed in a DMSO solution containing 1 mM SAM monomers for 1 h at room temperature. We used two types of SAM monomers that mimicked the electrically charged side chains of amino acids (Fig. 1b). 3-MPA and 2-MEA were used as mimics of the negatively charged and positively charged side chains, respectively. Finally, the SAM-functionalized electrodes were rinsed with IPA and Milli-Q water.

Surface characterization of the SAM-modified electrodes

Elemental analyses of the Au surfaces modified with SAM-functionalized Au electrodes were performed using X-ray photoelectron spectroscopy (XPS). The changes in the work function of the Au electrodes with and without each SAM were evaluated using photoemission yield spectroscopy in air (PYSA). Quartz crystal microbalance (QCM) measurements were performed to evaluate the molecular density of the SAMs on the Au surfaces. The adsorption of SAMs was evaluated based on the change in frequency when solutions of 0 or 1 mM amino acid derivatives in DMSO were passed.

The base frequency for the QCM measurements was defined to be 8.9 MHz.

Electrical detection of AAIs using the SAM-modified electrodes

After functionalization of the extended-gate sensing electrode, the FET sensor chip was connected to the measuring equipment (BCT-II, BioCMOS Co., Ltd.). An Ag/AgCl reference electrode with an inner solution of 3 M NaCl (RE-3VT, BAS Inc.) was also coupled with the measurement equipment as a control-gate electrode (Fig. 1c). First, a MOPS buffer solution (10 mM, pH 7.0) containing 1 or 10 mM electrolyte (NaCl or $CaCl_2$) was applied to the FET sensor chip. The change in the output voltage with time because of the fluctuation in electrode potential in the buffer solution was measured.[30] The drift of the output voltage was almost stabilized after 2 h. Hence, the device was incubated with the buffer solution for 2 h. The drift fraction was formulated to analyze the output voltage as a sensing signal (Fig. S1a†). Then, the change in output voltage (V_{OUT}) was measured while titrating the amino acid solution containing 0–10 μM amino acid and 1 or 10 mM electrolyte in 10 mM MOPS (pH 7.0) (Fig. S1b†). Calibrated V_{OUT} was determined by subtracting the drift fraction from the measured V_{OUT} (Fig. S1c†). All the electrical measurements were performed at room temperature. The V_{OUT} was determined from 42 independent detection points on SAMs, and the mean and standard error of 42 data were calculated.

Results

Chemical composition of the amino acid-mimicking SAMs

To confirm the immobilization of the amino acid-mimicking SAMs on the Au surface, we first performed an elemental analysis of the SAMs using XPS (Fig. 2). Compositional changes in the SAM systems on the Au surfaces were observed as shifts in each elemental peak of the amino acid derivatives in the C 1s, O 1s, N 1s, and S 2p regions. The C 1s peak at approximately 285 eV for each SAM could be imputed to the carbon attached to the sulfur atom. In addition, the C 1s peak at approximately 288 eV and the O 1s peak at approximately 533 eV in 3-MPA modified SAM could be imputed to the carbon and oxygen in the carboxyl group (Fig. 2a). The N 1s peak at approximately 400 eV in the 2-MEA modified SAM could be imputed to the nitrogen in the amino group (Fig. 2b). The peaks derived from the orbital doublets of S $2p_{3/2}$ (~162 eV) and S $2p_{1/2}$ (~163 eV) could be imputed to the sulfur in the thiol group. Notably, the changes in the peak ratios between S $2p_{3/2}$ and S $2p_{1/2}$ of each SAM were obtained (Fig. S2a and b†), which could be assigned to the presence of small amounts of disulfide-like compounds on the Au film. Based on the peak separation analysis in the S 2p region, the presence of disulfide-like compounds was more for 3-MPA than for 2-MEA, and that of thiol-derived compounds was more for 2-MEA than for 3-MPA. These results suggest that each amino acid derivative was adsorbed onto the Au surface, and the intermolecular distance of thiol groups on SAMs was shorter for 3-MPA than for 2-MEA.

We then performed PYSA measurements to confirm the donor or acceptor properties of the Au surfaces (Fig. 3). These properties of the Au surfaces were determined from a shift in the work function. The work function of the untreated SAM was 4.83 ± 0.02 eV. After 3-MPA modification, the work function shifted to 4.92 ± 0.01 eV, suggesting the presence of electron-withdrawing substituents (–COOH). In contrast, the work function of the Au film shifted to 4.71 ± 0.01 eV after modification of the film with 2-MEA, indicating the presence of electron-donating substituents ($-NH_2$) on the Au film. Notably, 3-MPA modification reduced the photoelectron yield from the Au surface. The dense adsorption of 3-MPA on the Au surface could inhibit the emission of photoelectrons.

Finally, we evaluated the density of the amino acid derivatives on the Au surfaces using QCM measurements (Table 1). Frequency changes (Δf) and molecular densities (ρ) were similar to those reported previously.[31,32] The ρ of 3-MPA on the Au surface was approximately 2.4-times higher than that of 2-MEA. 3-MPA forms hydrogen bonds between the carboxyl groups,[33] probably resulting in a denser adsorption than does 2-MEA. Based on the density and the interaction of

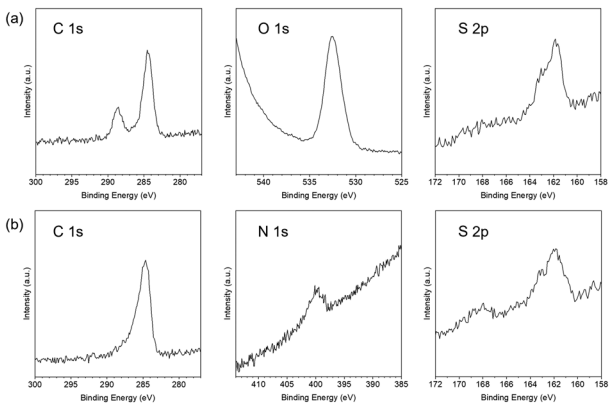

Fig. 2 X-ray photoelectron spectroscopy of C 1s, O 1s, N 1s, and S 2p regions of the Au film modified with (a) 3-mercaptopropionic acid or (b) 2-mercaptoethylamine monolayers.

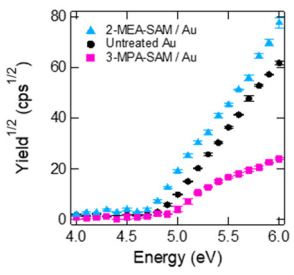

Fig. 3 Result of photoemission yield spectroscopy in air of the Au electrodes. Untreated Au (black), 3-mercaptopropionic acid (3-MPA)-treated Au (pink), and 2-mercaptoethylamine (2-MEA)-treated Au (blue). Error bars represent the standard errors of three measurements.

Table 1 Amounts of amino acid derivatives on the Au surface determined using the quartz crystal microbalance

SAM monomer	Δf (Hz)	Δm (ng)	ρ (nmol cm^{-2})
3-MPA	40.38 ± 1.21	44.22 ± 1.33	2.13 ± 0.06
2-MEA	12.44 ± 0.77	13.62 ± 0.85	0.90 ± 0.06

The weights of the SAM monomers on the Au surface were calculated from the frequency change.[34] The sensing area of the Au surface was 0.196 cm^2. Values represent the mean and standard error of three measurements. SAM, self-assembled monolayer; 2-MEA, 2-mercaptoethylamine; 3-MPA, 3-mercaptopropionic acid.

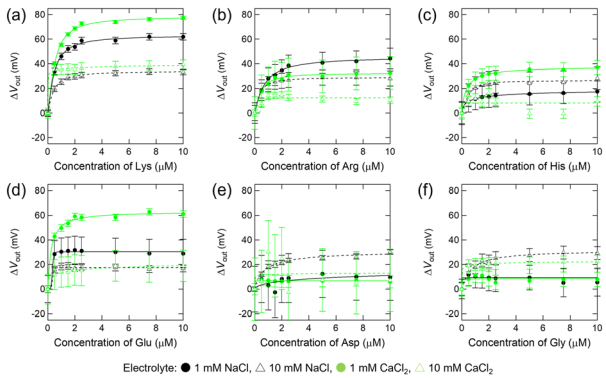

Fig. 4 Electrical detection of amino acids using the field-effect transistor sensor modified with the anionic monolayer (3-mercaptopropionic acid-self-assembled monolayer). Changes in the output voltage upon addition of Lys (a), Arg (b), His (c), Glu (d), Asp (e), or Gly (f) to the 3-morpholinopropanesulfonic acid buffer solution (10 mM) with 1 or 10 mM electrolyte (NaCl or $CaCl_2$) at pH 7.0. [Analyte] = 0–10 μM.

ligand molecules, 3-MPA could stand on the gold surface due to unlikely interaction between the carboxyl group and the gold. On the other hand, 2-MEA could lie on the gold surface due to the interaction between the amino group and the gold. Collectively, the XPS, PYSA, and QCM results showed that 3-MPA and 2-MEA were certainly adsorbed on the Au surface and that the alignment patterns varied depending on the molecule (Fig. S2c and d†). Moreover, these results suggested the formation of a monolayer on the Au surface, hence the thickness of the SAMs would be about the length of a 3-MPA or 2-MEA molecule.

Electrical detection of AAIs using amino acid-mimicking SAMs

First, we investigated the interactions between free amino acids and the negatively charged amino acid assembled on the Au electrode. Fig. 4 shows the relationship between the concentration of free amino acids and the changes in the output voltage (V_{OUT}) of the 3-MPA-modified FET device. In titration experiments with cationic amino acids (Lys, Arg, and His), concentration-dependent responses were observed (Fig. 4a–c). Based on the titration isotherms for these analytes, the apparent dissociation constant (K_d) for each titration experiment was estimated using the Hill–Waud model (Table 2). Considering the pH of the analyte solution (pH 7.0) and the pK_a values of 3-MPA, Lys, Arg, and His (Fig. 1), the electrical responses obtained in these titrations are attributed to electrostatic interactions between 3-MPA and the cationic amino acids. In contrast, the electrical responses to the anionic amino acids (Glu and Asp) were weaker than those to the cationic amino acids (Lys, Arg, and His) (Fig. 4d and e and Table 2). This is presumably due to the electrostatic repulsion between the carboxy moieties of 3-MPA and the carboxy–oxygens of Glu and Asp (*cf.* pK_a in Fig. 1). In particular, the lower response of the device to Gly (Fig. 4f and Table 2) indicated that the positively charged amino group in the main chain of the amino acids was insufficient to interact with the 3-MPA assembled on the Au surface.

Next, we examined the interactions between amino acids and positively charged amino acid-mimicking molecules. Fig. 5 illustrates the relationship between the concentration of amino acids and the changes in the V_{OUT} of the 2-MEA-modified FET device. Concentration-dependent responses were observed in the group of cationic amino acids as well as anionic amino acids (Lys, Arg, Glu, and Asp), and K_d was calculated (Fig. 5 and Table 3). The lower response of the device to Gly (Fig. 5f and Table 3) indicated that the negatively charged carboxyl groups in the main chain of the amino acids were probably insufficient to interact with the 2-MEA assembled on the Au surface. Considering the pH of the analyte solution (pH 7.0) and the pK_a values of Glu, Asp, and 2-MEA (Fig. 1), the interaction between 2-MEA and the anionic amino acids is probably driven by electrostatic interactions. In contrast, based on the pK_a values of Lys,

Table 2 Apparent dissociation constants (K_d/μM) obtained using the 3-mercaptopropionic acid-modified self-assembled monolayer

	Electrolyte in the analyte solution			
Amino acid	1 mM NaCl	10 mM NaCl	1 mM $CaCl_2$	10 mM $CaCl_2$
Lys	0.45 ± 0.03	0.39 ± 0.02	0.49 ± 0.02	ND[b]
Arg	0.70 ± 0.05	0.33 ± 0.02	0.44 ± 0.05	ND[a]
His	0.66 ± 0.16	0.44 ± 0.05	0.34 ± 0.02	ND[a]
Glu	ND[a]	ND[b]	0.25 ± 0.05	ND[b]
Asp	ND[a]	0.77 ± 0.16	ND[a]	ND[a]
Gly	ND[a]	0.70 ± 0.08	ND[a]	ND[b]

The apparent K_d values were calculated using the fitting calculation based on the Hill–Waud model[35] upon addition of each amino acid to 10 mM 3-morpholinopropanesulfonic acid buffer solution with 1 or 10 mM electrolyte (NaCl or $CaCl_2$) at pH 7.0. [a] ND indicates a low correlation between the concentration and voltage ($R^2 < 0.7$). [b] ND indicates that the error region is higher than the value.

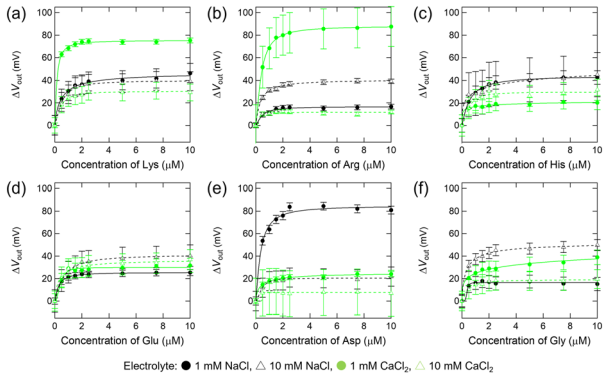

Fig. 5 Electrical detection of amino acids using the field-effect transistor sensor modified with the cationic monolayer (2-mercaptoethylamine-self-assembled monolayer). Changes in the output voltage upon addition of Lys (a), Arg (b), His (c), Glu (d), Asp (e), or Gly (f) to the 3-morpholinopropanesulfonic acid buffer solution (10 mM) with 1 or 10 mM electrolyte (NaCl or $CaCl_2$) at pH 7.0. [Analyte] = 0–10 μM.

Arg, and 2-MEA (Fig. 1), the interaction between 2-MEA and the cationic amino acids could be unique reactions *via* amino groups.[36]

Electrolyte effects on amino acid interactions

Finally, we investigated the effect of the added electrolyte on the interaction between the amino acids and SAM-modified FETs (Fig. 6). The image of charges of SAMs depending on the electrolyte concentration is shown in Fig. S3.† When the 3-MPA-SAM was used, the K_d values of Lys, Arg and His decreased with increasing ionic strength (Table 2), indicating higher affinities of these amino acids for the assembled carboxyl groups (3-MPA-SAM). These amino acids can easily form chelating complexes with metal cations,[37] indicating that the obtained affinity can be attributed to the complexation of these amino acids with each other *via* alkali- or alkaline earth metals (Na^+ or Ca^{2+}).[38,39] However, in the case of high ionic strength, such as in the presence of 10 mM $CaCl_2$, the response could be poor owing to strong electrostatic shielding. Interestingly, the lowest K_d value was obtained for Glu in the 1 mM $CaCl_2$ solution (Table 2). As carboxylic acids containing long alkyl groups readily form Ca^{2+}-mediated crosslinked structures,[40] the affinity between Glu and 3-MPA could be increased by Ca^{2+}-mediated crosslinking.

In the titration experiments on the 2-MEA-SAM, the K_d of Glu increased with increasing ionic strength (Table 3). This indicated that the carboxy moiety in these amino acids preferentially interacts with Na^+ or Ca^{2+}, resulting in a lower affinity between the amino-terminated group on the 2-MEA-SAM and the carboxy moiety in the amino acids. However, increasing the ionic strength and K_d of Lys, Arg, and Asp resulted in little change, indicating that the affinity of these amino acids for 2-MEA was not ion-sensitive (Table 3). Unlike the 3-MPA-modified SAM, the 2-MEA-modified SAM showed a concentration-dependent response at high ionic strength, such as in the presence of 10 mM $CaCl_2$ (Fig. 4 and 5). The contribution of the electrostatic interactions to the electrical response was probably less for the amine-modified SAM than for the carboxylic acid-modified SAM (Fig. 6).

We finally consider not only the direct intervention of electrolytes in the AAIs, but also the indirect intervention of electrolytes in relation to the Hofmeister series.[41] In general, the salting-out effect is said to be stronger for Na^+ than for Ca^{2+}, meaning that van der Waals attraction and hydrophobic interactions between AAIs are stronger in the presence of Na^+ compared to Ca^{2+}. However, the Hofmeister series can be reversed depending on the charge and hydrophobicity of the interaction surface; for example, that of cations is reversed at positively charged interfaces.[42] This implies that van der Waals attraction and hydrophobic interactions are more effective in the presence of Ca^{2+} on the 2-MEA-SAM. Thus, Lys with a long alkyl chain would likely exhibit a lower K_d value under such conditions due to hydrophobic interactions (Table 3).

Discussion

We presented an analytical model for AAIs using electrical detection on the Au surface. Since the K_d depends on the ionic strength and the type of molecule with different pK_a values (Tables 2 and 3), the electrostatic AAIs could mainly be evaluated. Because approximately 0.1 mL of 0–10 μM amino acid solution was flowed over the Au surface on which amino acid derivatives in nmol order were adsorbed, we could observe interaction among nmol-order molecules. Solubility

Table 3 Apparent dissociation constants (K_d/μM) obtained using the 2-mercaptoethylamine-modified self-assembled monolayer

	Electrolyte in the analyte solution			
Amino acid	1 mM NaCl	10 mM NaCl	1 mM $CaCl_2$	10 mM $CaCl_2$
Lys	0.49 ± 0.07	0.49 ± 0.03	0.15 ± 0.04	0.37 ± 0.04
Arg	0.44 ± 0.08	0.33 ± 0.03	0.39 ± 0.01	ND[a]
His	0.56 ± 0.02	ND[b]	ND[b]	0.48 ± 0.08
Glu	0.26 ± 0.02	0.63 ± 0.03	0.40 ± 0.06	0.32 ± 0.06
Asp	0.35 ± 0.06	0.41 ± 0.05	0.34 ± 0.06	ND[a]
Gly	ND[a]	0.31 ± 0.03	ND[b]	0.44 ± 0.05

The apparent K_d values were calculated using the fitting calculation based on the Hill–Waud model[35] upon addition of each amino acid to 10 mM 3-morpholinopropanesulfonic acid buffer solution with 1 or 10 mM electrolyte (NaCl or $CaCl_2$) at pH 7.0. [a] ND indicates a low correlation between the concentration and voltage ($R^2 < 0.7$). [b] ND indicates that the error region is higher than the value.

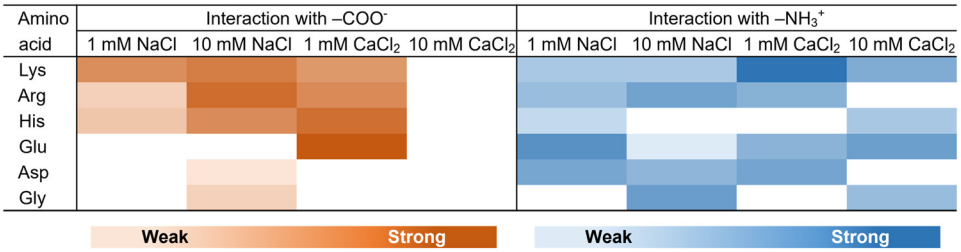

Fig. 6 Heat map of the interactions depending on the ionic strength and the type of molecule based on the dissociation constant (Tables 2 and 3). White areas represent that the interactions could not be properly evaluated.

experiments are used for evaluating AAIs, but they can only detect millimolar to molar order interactions, and the AAIs may depend on solvent properties, such as viscosity and pH.[43,44] Computational simulations have been used to evaluate the AAIs in the protein structure and in solution,[16,45] but the spatial and temporal scale restrictions were severe, and many approximations had to be introduced. One feature of our system is the on-site evaluation of AAIs at low molecular concentrations, where AAIs are barely affected by solvent properties, without any approximation or constraints.

In this study, two types of SAMs with different surface charges were prepared. Based on XPS, PYSA, and QCM analyses, the negatively charged 3-MPA-SAM showed a higher molecular density on the Au surface than did the positively charged 2-MEA-SAM on the same surface. This indicated that the intermolecular distance of the carboxy-terminated group (3-MPA) in the SAM was shorter than that of the amine-terminated group (2-MEA) in the SAM (Fig. S2 and Table 1). In other words, the amount of Au exposed on the SAM was probably smaller for 3-MPA than for 2-MEA. In our SAM system, 3-MPA selectively responded to cationic amino acids, whereas 2-MEA did not (Fig. 4 and 5). Considering previous reports on the nonspecific adsorption of amino acids onto bare Au,[46] in the case of the 2-MEA-SAM, the affinity between Au and amino acids as well as the interaction between 2-MEA and amino acids could be represented as responses. Thiol molecules containing long-chain alkyl groups easily accumulate on the Au surface.[47,48] In the future, SAMs should be modified with such molecules to evaluate the interaction between amino acids and assembled amines without affinity between amino acids and Au.

Considering PPIs, our findings regarding the differences in the selectivity of interactions and the degree of molecular accumulation have interesting implications. 3-MPA, a mimic of the Glu side chain, and 2-MEA, a mimic of the Lys side chain, were modified on the Au surface. Cationic amino acids interacted selectively in the Glu-assembled region, whereas all amino acids interacted non-selectively in the Lys-assembled region (Fig. 6). Proteins abundant in charged amino acids interact with each other and form protein assemblies, such as droplets and aggregates.[26,49] Notably, Glu-rich proteins tend to drive protein assembly formation, whereas Lys-rich proteins tend to be incorporated into protein assemblies.[50] In view of our results, Glu-rich regions would lead to selective interactions with certain proteins, resulting in the formation of protein assemblies with different compositions. In contrast, Lys-rich regions might be easily incorporated into various protein assemblies through nonselective interactions. Based on the protein data bank, in the distribution of amino acids in protein conformations, the abundance of Glu is greater than that of Lys in the folded structure, whereas it is the opposite in the disordered structure.[51,52] Because the Glu side chain assembles more easily than the Lys side chain (Table 1), Glu is probably more involved in the compact protein structure than Lys. Our observations on the assembly propensity of amino acid side chains are significant for reconsidering protein folding. Moreover, amine compounds inhibit the inactivation and aggregation of proteins, but the underlying mechanisms for these effects remain unelucidated.[53,54] We observed nonselective interactions of amino groups (Fig. 6), possibly describing the potential for inhibition of PPIs by amine compounds. Our system can be used to explore new compounds that inhibit PPIs.

Conclusions

We established an experimental model and analytical platform for the evaluation of AAIs using a FET-based sensor functionalized with amino acid-mimicking monolayers. Using this system, the interactions between charged amino acids and accumulated side chains were detected in nmol order based on electrical responses. Interestingly, cationic amino acids responded selectively to carboxylic acid-accumulated monolayers, whereas all amino acids responded non-selectively to amine-accumulated monolayers. The slight difference in the molecular structure of the SAM probably contributed to the change in the interaction. In addition, we could also evaluate the differences in AAIs as a function of ionic strength. We believe that the applicability of this model could be expanded to the analysis of not only other AAIs governing PPIs but also non-specific interactions between proteins and small molecules.

Data availability

The data supporting this article have been included as part of the ESI.†

Author contributions

A. N.: conceptualization, investigation, writing – original draft. K. S.: conceptualization, supervision. T. M.: investigation, methodology, supervision. All authors: writing – review and editing.

Conflicts of interest

There are no conflicts to declare.

Acknowledgements

A part of this study was conducted at the AIST Nano-Processing Facility, supported by the "Nanotechnology Platform Program" of the Ministry of Education, Culture, Sports, Science and Technology (MEXT), Japan. We acknowledge BioCMOS Co., Ltd. and Mitorika Co., Ltd. for preparing and supplying the FET sensor array chip. We would also like to thank Dr. H. Sugai for useful discussions on the selection of SAMs that mimic the electrically charged side chains of amino acids. We gratefully acknowledge financial support provided by the Japan Science and Technology Agency, Precursory Research for Embryonic Science and Technology (JST PRESTO) program (Grant No. JPMJPR21RB), the Japan Society for the Promotion of Science (JSPS) KAKENHI (Grant No. 22K19284, 23KJ0259), the Tanaka Kikinzoku Memorial Foundation, and the Fuji Seal Foundation, and a special strategic grant from AIST.

Notes and references

1 J. Zhu, N. Avakyan, A. Kakkis, A. M. Hoffnagle, K. Han, Y. Li, Z. Zhang, T. S. Choi, Y. Na, C.-J. Yu and F. A. Tezcan, *Chem. Rev.*, 2021, **121**, 13701–13796.
2 V. N. Uversky, *Curr. Opin. Struct. Biol.*, 2017, **44**, 18–30.
3 S. F. Banani, H. O. Lee, A. A. Hyman and M. K. Rosen, *Nat. Rev. Mol. Cell Biol.*, 2017, **18**, 285–298.
4 R. Kumar, S. Singh and O. V. Singh, *J. Ind. Microbiol. Biotechnol.*, 2008, **35**, 377–391.
5 J. A. Wells and C. L. McClendon, *Nature*, 2007, **450**, 1001–1009.
6 I. M. A. Nooren and J. M. Thornton, *EMBO J.*, 2003, **22**, 3486–3492.
7 G. L. Dignon, R. B. Best and J. Mittal, *Annu. Rev. Phys. Chem.*, 2020, **71**, 53–75.
8 V. S. Rao, K. Srinivas, G. N. Sujini and G. N. S. Kumar, *Int. J. Proteomics*, 2014, **2014**, 147648.
9 M. M. Pierce, C. S. Raman and B. T. Nall, *Methods*, 1999, **19**, 213–221.
10 J. Vaynberg and J. Qin, *Trends Biotechnol.*, 2006, **24**, 22–27.
11 B. Causier and B. Davies, *Plant Mol. Biol.*, 2002, **50**, 855–870.
12 D. W. Piston and G.-J. Kremers, *Trends Biochem. Sci.*, 2007, **32**, 407–414.
13 G. T. Valente, M. L. Acencio, C. Martins and N. Lemke, *PLoS One*, 2013, **8**, e65587.
14 C. Prieto and J. De Las Rivas, *Nucleic Acids Res.*, 2006, **34**, W298–W302.
15 C. Stark, B.-J. Breitkreutz, T. Reguly, L. Boucher, A. Breitkreutz and M. Tyers, *Nucleic Acids Res.*, 2006, **34**, D535–D539.
16 K. Kamagata, M. Ariefai, H. Takahashi, A. Hando, D. R. G. Subekti, K. Ikeda, A. Hirano and T. Kameda, *Sci. Rep.*, 2022, **12**, 13718.
17 K. A. Burke, A. M. Janke, C. L. Rhine and N. L. Fawzi, *Mol. Cell*, 2015, **60**, 231–241.
18 T. Minamiki, Y. Ichikawa and R. Kurita, *Sensors*, 2020, **20**, 1–28.
19 T. Minami, T. Minamiki and Y. Sasaki, *Electrochemistry*, 2018, **86**, 303–308.
20 S. M. Patrie and M. Mrksich, *Anal. Chem.*, 2007, **79**, 5878–5887.
21 P. Didier, N. Lobato-Dauzier, N. Clément, A. J. Genot, Y. Sasaki, É. Leclerc, T. Minamiki, Y. Sakai, T. Fujii and T. Minami, *ChemElectroChem*, 2020, **7**, 1332–1336.
22 M. Wipf, R. L. Stoop, A. Tarasov, K. Bedner, W. Fu, I. A. Wright, C. J. Martin, E. C. Constable, M. Calame and C. Schönenberger, *ACS Nano*, 2013, **7**, 5978–5983.
23 T. Minamiki, Y. Ichikawa and R. Kurita, *ACS Appl. Mater. Interfaces*, 2020, **12**, 15903–15910.
24 N. Crivillers, E. Orgiu, F. Reinders, M. Mayor and P. Samorì, *Adv. Mater.*, 2011, **23**, 1447–1452.
25 R. M. Kramer, V. R. Shende, N. Motl, C. N. Pace and J. M. Scholtz, *Biophys. J.*, 2012, **102**, 1907–1915.
26 S. Xue, R. Gong, F. He, Y. Li, Y. Wang, T. Tan and S.-Z. Luo, *Sci. Adv.*, 2019, **5**, eaax5349.
27 M. Idrees, A. R. Mohammad, N. Karodia and A. Rahman, *Antibiotics*, 2020, **9**, 1–23.
28 N. Shambetova, Y. Chen, H. Xu, L. Li, J. Solandt, Y. Zhou, J. Wang, H. Su, H. Brismar and Y. Fu, *J. Phys. Chem. C*, 2016, **120**, 3519–3529.
29 P. H. Connett and K. E. Wetterhahn, *J. Am. Chem. Soc.*, 1986, **108**, 1842–1847.
30 T. Kajisa and T. Sakata, *Jpn. J. Appl. Phys.*, 2015, **54**, 04DL06.
31 J. J. Chance and W. C. Purdy, *Thin Solid Films*, 1998, **335**, 237–244.
32 X. Huang, J. Xu, H.-F. Ji, G. Li and H. Chen, *Anal. Methods*, 2014, **6**, 4530–4536.
33 A. Kudelski, *Surf. Sci.*, 2002, **502–503**, 219–223.
34 H. Sota, H. Yoshimine, R. F. Whittier, M. Gotoh, Y. Shinohara, Y. Hasegawa and Y. Okahata, *Anal. Chem.*, 2002, **74**, 3592–3598.
35 J. Shi, T. Yang, S. Kataoka, Y. Zhang, A. J. Diaz and P. S. Cremer, *J. Am. Chem. Soc.*, 2007, **129**, 5954–5961.
36 Y. K. Ng and L. Konermann, *J. Am. Chem. Soc.*, 2024, **146**, 8394–8406.
37 Y. Shimazaki, M. Takani and O. Yamauchi, *Dalton Trans.*, 2009, 7854–7869.
38 H. D. M. Pham, G. C. Boles and P. B. Armentrout, *J. Phys. Chem. A*, 2021, **125**, 6332–6347.
39 N. Tang and L. H. Skibsted, *J. Agric. Food Chem.*, 2016, **64**, 4376–4389.

40 S. Peng and C. Wu, *Macromolecules*, 1999, **32**, 585–589.
41 H. I. Okur, J. Hladílková, K. B. Rembert, Y. Cho, J. Heyda, J. Dzubiella, P. S. Cremer and P. Jungwirth, *J. Phys. Chem. B*, 2017, **121**, 1997–2014.
42 N. Schwierz, D. Horinek, U. Sivan and R. R. Netz, *Curr. Opin. Colloid Interface Sci.*, 2016, **23**, 10–18.
43 L. A. Ferreira, V. N. Uversky and B. Y. Zaslavsky, *J. Mol. Liq.*, 2019, **277**, 123–131.
44 A. Nomoto, S. Nishinami and K. Shiraki, *Biophys. Chem.*, 2022, **287**, 106831.
45 C. Nacar, *Protein J.*, 2020, **39**, 21–32.
46 D. Biriukov and Z. Futera, *J. Phys. Chem. C*, 2021, **125**, 7856–7867.
47 K. Konno, E. Ito, J. Noh and M. Hara, *Jpn. J. Appl. Phys.*, 2006, **45**, 405.
48 E. Bedford, V. Humblot, C. Méthivier, C.-M. Pradier, F. Gu, F. Tielens and S. Boujday, *Chem. – Eur. J.*, 2015, **21**, 14555–14561.
49 S. Ambadipudi, J. Biernat, D. Riedel, E. Mandelkow and M. Zweckstetter, *Nat. Commun.*, 2017, **8**, 275.
50 M. Hardenberg, A. Horvath, V. Ambrus, M. Fuxreiter and M. Vendruscolo, *Proc. Natl. Acad. Sci. U. S. A.*, 2020, **117**, 33254–33262.
51 S. M. Cascarina, M. R. Elder and E. D. Ross, *PLoS Comput. Biol.*, 2020, **16**, e1007487.
52 P. Y. Chou and G. D. Fasman, *Biochemistry*, 1974, **13**, 211–222.
53 M. Kudou, K. Shiraki, S. Fujiwara, T. Imanaka and M. Takagi, *Eur. J. Biochem.*, 2003, **270**, 4547–4554.
54 A. J. Michael, *J. Biol. Chem.*, 2018, **293**, 18693–18701.